Journal of Power Sources 273 (2015) 185–195

Contents lists available at ScienceDirect

Journal of Power Sources

journal homepage: www.elsevier.com/locate/jpowsour

A battery chemistry-adaptive fuel gauge using probabilistic data association

G.V. Avvari, B. Balasingam*, K.R. Pattipati, Y. Bar-Shalom

Department of Electrical and Computer Engineering, University of Connecticut, 371 Fairfield Way, U-2157, Storrs, CT 06269, USA

HIGHLIGHTS

- A chemistry adaptive battery fuel gauge is derived based on the PDA algorithm.
- The PDA algorithm selects the correct OCV curve online from a library.
- For unknown batteries, the PDA-BFG selects the most similar OCV curve.
- A machine learning approach selects diverse OCV curves to fill the library.

ARTICLE INFO

Article history:
Received 21 May 2014
Received in revised form
15 August 2014
Accepted 2 September 2014
Available online 16 September 2014

Keywords:
Li-ion batteries
Battery fuel gauging (BFG)
State of charge (SOC)
OCV characterization
New battery detection
Probabilistic data association (PDA)

ABSTRACT

This paper considers the problem of state of charge (SOC) tracking in Li-ion batteries when the battery chemistry is unknown. It is desirable for a battery fuel gauge (BFG) to be able to perform without any offline characterization or calibration on sample batteries. All the existing approaches for battery fuel gauging require at least one set of parameters, a set of open circuit voltage (OCV) parameters, that need to be estimated offline. Further, a BFG with parameters from offline characterization will be accurate only for a "known" battery chemistry. A more desirable BFG is one that is accurate for "any" battery chemistry. In this paper, we show that by storing finite sets of OCV parameters of possible batteries, we can derive a generalized BFG using the probabilistic data association (PDA) algorithm. The PDA algorithm starts by assigning prior model probabilities (typically equal) for all the possible models in the library and recursively updates those probabilities based on the voltage and current measurements. In the event of an unknown battery to be gauged, the PDA algorithm selects the most similar OCV model to the battery from the library. We also demonstrate a strategy to select the minimum sets of OCV parameters representing a large number of Li-ion batteries. The proposed approaches are demonstrated using data from portable Li-ion batteries.

1. Introduction

Rechargeable batteries have increasingly been finding applications in many emerging frontiers; consumer electronics, aerospace equipment, electric vehicles and smart grid are some examples. Lithium-ion and lithium-polymer based rechargeable batteries are widely adopted due to their high energy density and long life. Battery fuel gauging (BFG) plays an important role in rechargeable battery applications. A BFG tracks the state of charge (SOC) and state of health (SOH) of the battery and predicts the time to shut down (TTS) and the remaining useful life (RUL).

Li-ion/polymer batteries are being produced by numerous manufacturers and the exact chemistry of these batteries is usually not available (mostly) due to proprietary reasons. In the current business practice, battery manufacturers do not provide BFG capabilities — it is up to the device manufacturer to develop the BFG which, in the present state of the art, requires some parameters that are battery specific. Further, owing to the fact that the battery characteristics drift with environmental and usage factors, a BFG should have the ability to perform independently of the manufacturer data-sheets. A robust BFG capability allows an end user to rapidly switch batteries without requiring the user to adhere to a particular battery manufacturer. This is particularly useful in portable electronic applications where battery swaps are frequent.

* Corresponding author. Tel./fax: +18604865376.
E-mail addresses: vinod@engr.uconn.edu (G.V. Avvari), bala@engr.uconn.edu, bhalakumar@gmail.com (B. Balasingam), krishna@engr.uconn.edu (K.R. Pattipati), ybs@engr.uconn.edu (Y. Bar-Shalom).

http://dx.doi.org/10.1016/j.jpowsour.2014.09.006
0378-7753/

Nomenclature

$\mathbf{a}[k]$	battery equivalent (*voltage drop*) model (see (2))
$\mathbf{b}$	battery equivalent model parameter (2)
BFG	battery fuel gauge
c_h	Coulomb counting coefficient (1)
$H^j[k]$	derivative of OCV a (6)
$\mathbf{k}_j$	OCV parameters of the j^{th} model (2)
$n_d[k]$	measurement noise of the *voltage drop* model (2)
OCV	open circuit voltage
$\mathbf{p}^T(x_s[k])$	OCV model (2)
Q	process noise variance (1)
R	measurement noise variance (of the voltage drop model) (2)
$\mathcal{L}^j[k]$	likelihood of j^{th} model at time k (14)
SOC	state of charge
$w_s[k]$	process noise (1)
$W^j[k]$	Kalman filter gain corresponding to model j (18)
$x_s[k]$	state of charge (SOC) of the battery (1)
$z_i[k]$	measured current through the battery (1)
$z_v[k]$	measured terminal voltage (2)
$\beta^j[k]$	probability of the j^{th} model at time k (13)
$\nu^j[k]$	Kalman filter innovation corresponding to model j (18)

Most of the existing BFG algorithms are based on an OCV model and a dynamic equivalent circuit model (ECM); the parameters of the OCV curve (shown to be unchanged over temperature changes and aging [1]) are estimated offline and the ECM parameters (known to vary with temperature, loading [2] and aging) are estimated online. In most works, (the *combined model* [3,4]) was adopted for modeling the OCV–SOC relationship; many other possible OCV models are discussed in Ref. [1] as well. In Refs. [3–8], different dynamic models such as simple (resistance only) model, zero/one state hysteresis mode and enhanced self correcting models are discussed; these works give significant attention to modeling the hysteresis effect in the battery. Combinations of resistance/capacitance models where the hysteresis effect is either ignored or modeled as an error can be found in Refs. [9–18].

Based on the application, BFG can be divided into two categories: those used in fixed applications and those used in portable applications. In fixed applications, the BFG has to continuously monitor only one battery (or pack), whereas in portable applications the BFG might be expected to monitor two (or more) batteries — one at a time. Table 1 compares the requirements of a BFG in fixed vs. mobile applications.

Our focus in this paper is on portable applications, although a generalized BFG will be useful in fixed applications as well.

Table 1
Comparison of BFG requirements in fixed vs. mobile applications.

Fixed applications	Portable applications
Load is constantly connected to the battery	Possibility for battery swap, e.g., a smart phone user keeping two batteries — one in use and one as back-up.
Battery is replaced after end of its life; BFG doesn't have to keep the parameters of the old battery.	Battery swap is practiced, i.e., the BFG needs to keep the parameters of two (or more) batteries. When a back-up battery is inserted, the BFG needs to adapt to the parameters as well.
Examples: electric vehicles (EV), power tools, aerospace equipment.	Examples: smart phones, wearable devices, tablets, laptops, etc.

An accurate BFG requires the offline estimation of several battery equivalent model parameters. Recently, we developed robust approaches for battery fuel gauging that require the characterization of only the open circuit voltage (OCV) of the battery SOC [19,2,20]. In Refs. [1], the many aspects of OCV parameter estimation of Li-ion battery cells are elaborated. Later in this paper, we show that the OCV parameters of several types of batteries can be reduced to few sets of OCV parameters though machine learning techniques.

There are two possible approaches to develop a generalized BFG that is independent of battery chemistry. The first approach is to simply have a library of OCV parameters and to employ online detection approaches in order to select the most suitable OCV model for fuel gauging. In other words, this first approach seeks to resolve the association ambiguity between several possible OCV parameters and the battery being monitored. The second approach seeks to estimate the OCV parameters from online data [21–23]; an iterative process is employed to continuously update the OCV parameters and battery capacity. One of the challenges faced by the second approach is the detection of new batteries (due to battery swaps) and restarting the OCV parameter estimation routine only when required. Further, the iterative estimation of SOC, OCV & ECM parameters and the battery capacity adds to the instability of the BFG algorithm and costs in terms of robustness.

The present paper takes the first approach to chemistry adaptive battery fuel gauging.[1] Currently, we are investigating the second approach as well. To the knowledge of the authors, no other work has attempted to develop a generalized BFG that adapts to battery chemistries online. The contributions of this paper are listed below:

1. *Derivation of a generalized BFG based on PDA*. We derive a novel approach to chemistry-adaptive battery fuel gauging based on the principles of probabilistic data association [24]. As the name suggests, the PDA assesses the probability of each known OCV model against the observations (instantaneous voltage and current) and employs Gaussian mixture reduction technique to recursively propagate the best possible posterior probability density of the SOC.
2. *The PDA approach also can serve as a means to detect a new battery*. The association probability can also serve as a means to new battery detection, as far as the new battery significantly differs from the current battery in its OCV characteristics, capacity and resistance.
3. *The PDA algorithm enables the BFG to work on unknown batteries*. In the event that an unknown battery for which the OCV parameters do not belong to any of the ones in the library, the PDA algorithm will find the most similar OCV model from the library and use it to gauge the unknown battery; assuming that the library has a diverse set of OCV parameters, the PDA based BFG becomes applicable on unknown batteries.
4. *A clustering approach to store minimal set of OCV parameters to be used by the generalized BFG*. By exploiting machine learning techniques, we demonstrate a novel approach to select the minimal number of OCV models without compromising the SOC tracking performance.

The initial interest in developing universal battery solutions came from battery charger designers in order to address the ever increasing number of different types of battery operated equipment and each of these having its own customized charger; this increases the amount of electronic wastage and adds to the cost of the device. Hence, there has been significant effort in developing a *universal*

[1] The second, online OCV estimation approach is left for future investigation.

battery charger [25–28]. In the most simplest form, the first challenge in designing a universal charger is to find the voltage to which the battery has to be charged. The approaches in Refs. [25–28] suggest using a look-up table of incremental voltage in response to charging by a certain number of Coulombs.

It must be noted that the universal charging approaches discussed in Refs. [25–28] attempt to charge the battery in a very simple form – finding the correct voltage to apply. The optimal battery charging is an entirely different problem (see Refs. [29–31] and the references therein) which aims to apply optimal charging waveform to the battery such that the charging time can be reduced without affecting the longevity of the battery.[2] The optimal charging algorithm (OCA) also requires accurate knowledge of the battery SOC which makes BFG capability a requirement in OCAs. Our focus on this paper is limited to developing a chemistry adaptive BFG.

The rest of this paper is organized as follows: In section 2, we develop the PDA algorithm for the robust multimodel BFG with many possible OCV model parameters. In section 3, we show how to select the right OCV parameter set for storage from among many possible candidates. Computer simulations of the proposed approaches are presented in section 4 based on simulated data as well as real battery data and the paper is concluded in section 5.

2. PDA approach for robust multimodel BFG

The SOC tracking problem [19,2,20] with multiple models for the OCV parameter set is summarized below:

$$x_s[k] = x_s[k-1] + c_h \Delta z_i[k-1] + w_s[k] \tag{1}$$

$$\begin{aligned} z_v[k] &= V_o^j(x_s[k]) + \mathbf{a}^T[k]\mathbf{b} + n_d[k] \\ &= \mathbf{p}^T(x_s[k])\mathbf{k}_j + \mathbf{a}^T[k]\mathbf{b} + n_d[k] \quad j = 1,\ldots,N_j \end{aligned} \tag{2}$$

where $x_s[k]$ is the SOC of the battery, c_h is the Coulomb counting coefficient [2], Δ is the sampling time, $z_v[k]$ is the measured voltage, $z_i[k]$ is the measured current, $w_s[k]$ and $n_d[k]$ are the process and measurement noises (see Ref. [20] for description), which are assumed to be zero-mean white with standard deviations $\sqrt{Q}$ and $\sqrt{R}$, respectively, $\mathbf{b}$ corresponds to the dynamic equivalent circuit model parameter vector (which has model dependent dimensions, see Ref. [19]), $\mathbf{a}$ is a known vector depending on the dynamic equivalent circuit model used, and the OCV model is given by

$$\mathbf{p}^T(x_s[k]) = \left[1 \;\; \frac{1}{x_s[k]} \;\; \frac{1}{(x_s[k])^2} \;\; \frac{1}{(x_s[k])^3} \;\; \frac{1}{(x_s[k])^4} \;\; x_s[k] \;\; \log(x_s[k]) \;\; \log(1-x_s[k])\right] \tag{3}$$

and the j^{th} set of OCV model parameters are given by

$$\mathbf{k}_j = \left[K_0^j K_1^j K_2^j K_3^j K_4^j K_5^j K_6^j K_7^j\right]^T \tag{4}$$

and

$$\mathbf{k}_j \in \left\{\mathbf{k}_1, \mathbf{k}_2, \ldots, \mathbf{k}_{N_j}\right\} \tag{5}$$

indicates N_j OCV model parameters.

The measurement model (2) can be written, to a first order approximation, as

$$\begin{aligned} z_v[k] &\approx V_o^j(\hat{x}_s[k|k-1]) + H^j[k](x_s[k] - \hat{x}_s[k|k-1]) + \mathbf{a}^T[k]\mathbf{b} \\ &\quad + n_d[k] = H^j[k]x_s[k] + e^j[k] + \mathbf{a}^T[k]\mathbf{b} + n_d[k] \end{aligned} \tag{6}$$

where

$$H^j[k] = \left.\frac{dV_o^j(x)}{dx}\right|_{x=\hat{x}_s[k|k-1]} \tag{7}$$

$$e^j[k] = V_o^j(\hat{x}_s[k|k-1]) - H^j[k]\hat{x}_s[k|k-1] \tag{8}$$

Given the measured voltage $z_v[k]$ and current $z_i[k]$, the objective is to recursively estimate the SOC $x_s[k]$.

Using Bayes rule, the posterior probability density of $x_s[k]$ given all the measurements up to k, $z_v[1{:}k]$, is written in (9)

$$\begin{aligned} p\left(x_s[k]|z_v[1:k]\right) &= \sum_{j=1}^{N_j} p(x_s[k]|j, z_v[1:k])p(j|z_v[1:k]) \\ &= \frac{\sum_{j=1}^{N_j} p(z_v[k]|x_s[k], j, z_v[1:k-1])p(j|z_v[1:k])p(x_s[k]|z_v[1:k-1])}{p(z_v[k]|z_v[1:k-1], j)} \end{aligned} \tag{9}$$

where the denominator is the normalizing factor and

$$\begin{aligned} &p\left(z_v[k]|x_s[k], j, z_v[1:k-1]\right) \\ &\quad = \mathcal{N}\left(z_v[k]; H^j[k]x_s[k] + e^j[k] + \mathbf{a}^T[k]\mathbf{b}, R\right) \end{aligned} \tag{10}$$

$$p\left(j|z_v[1:k]\right) \triangleq \beta^j[k] \tag{11}$$

$$p(x_s[k]|z_v[1:k-1]) = \mathcal{N}(x_s[k]; \hat{x}_s[k|k-1], P_s[k|k-1]) \tag{12}$$

The model probability[3] $\beta^j[k]$ is updated to its current value as.

$$\begin{aligned} \beta^j[k] &= p\left(j|z_v[1:k]\right) = \frac{p(z_v[k]|j, z_v[1:k-1])p(j|z_v[1:k-1])}{p(z_v[k]|z_v[1:k-1])} \\ &= \frac{p(z_v[k]|j, z_v[1:k-1])p(j|z_v[1:k-1])}{\sum_{j=1}^{N_j} p(z_v[k]|j, z_v[1:k-1])p(j|z_v[1:k-1])} \\ &= \frac{\mathcal{L}^j[k]\beta^j[k-1]}{\sum_{l=1}^{N_j} \mathcal{L}^l[k]\beta^l[k-1]} \end{aligned} \tag{13}$$

where

$$\begin{aligned} \mathcal{L}^j[k] \triangleq p\left(z_v[k]|j, z_v[1:k-1]\right) &= \mathcal{N}\left(z_v[k]; \hat{z}^j[k|k-1], S^j[k]\right) \\ &= \mathcal{N}\left(0; \nu^j[k], S^j[k]\right) \end{aligned} \tag{14}$$

is the likelihood of the OCV model j (specified by $\mathbf{k}_j$), and

$$\nu^j[k] = z_v[k] - z_v^j[k|k-1] \tag{15}$$

$$S^j[k] = \left(H^j[k]\right)^2 P_s[k|k-1] + R \tag{16}$$

[2] Fast charging ages the battery fast.

[3] In the PDAF for tracking in clutter [24] this is the (association) probability of measurement j originating from the target of interest; here, this is the probability that the (only) measurement originated form model j. Consequently, we use the designation of model probability.

are the innovation and the variance of the innovation, respectively.

Now, (9) is explicitly written as

$$p\left(x_s[k]|z_v[1:k]\right) = c\sum_{j=1}^{N_j}\beta^j[k]\mathcal{N}\left(z_v[k];H^j[k]x_s[k]+e^j[k],R\right)\cdot\mathcal{N}\left(x_s[k];\hat{x}_s[k|k-1],P_s[k|k-1]\right) = c\sum_{j=1}^{N_j}\beta^j[k]\mathcal{N}\left(x_s[k];\hat{x}^j[k|k],P_s^j[k|k]\right) \quad (17)$$

where c is the normalizing constant and

$$\hat{x}_s^j[k|k] = \hat{x}_s[k|k-1] + W^j[k]\nu^j[k] \quad (18)$$

$$P_s^j[k|k] = P_s[k|k-1] - \left(W^j[k]\right)^2 S^j[k] = \left(1-w^j[k]H^j[k]\right)^2 P_s[k|k-1] + w^j[k]^2 R \quad (19)$$

are the "mode matched" SOC estimates and the corresponding estimation error variances, and

$$W^j[k] = \frac{P_s[k|k-1]H^j[k]}{S^j[k]} \quad (20)$$

is the Kalman gain corresponding to the j^{th} model.

The posterior distribution $p(x_s[k]|z_v[1{:}k])$ becomes a Gaussian mixture as shown in (17). In recursive estimation, we seek to approximate this mixture as a single Gaussian component. There are several approaches for *Gaussian mixture reduction* in the literature, such as [32] and the references therein. It is shown in Refs. [[33],Theorem2] that, the Gaussian density $\mathcal{N}(x_s[k];\hat{x}_s[k|k],P_s[k|k])$ minimizes the Kullback-Leibler distance between (17) and its Gaussian approximation, where

$$\hat{x}_s[k|k] = \sum_{j=1}^{N_j}\beta^j[k]\hat{x}_s^j[k|k] = \hat{x}_s[k|k-1] + \sum_{j=1}^{N_j}\beta^j[k]W^j[k]\nu^j[k] \quad (21)$$

$$P_s[k|k] = \sum_{j=1}^{N_j}\beta^j[k]\left(P_s^j[k|k] + \left(\hat{x}_s^j[k|k]-\hat{x}_s[k|k]\right)^2\right) = \sum_{j=1}^{N_j}\beta^j[k]\left[P_s^j[k|k] + W^j[k]\left(\nu^j[k]-\bar{\nu}[k]\right)^2\right] \quad (22)$$

where

$$\bar{\nu}[k] = \sum_{j=1}^{N_j}\beta^j[k]W^j[k]\nu^j[k] \quad (23)$$

Now, starting from the SOC estimate $\hat{x}_s[k-1|k-1]$ and the corresponding estimation error variance $P_s[k-1|k-1]$, the updated SOC estimate $\hat{x}_s[k|k]$ and the corresponding estimation error variance $P_s[k|k]$ can be obtained as follows [34]:

First, the state prediction and the state prediction variance, both of which do not depend on the OCV models, are computed as.

Prediction $\hat{x}_s[k|k-1] = \hat{x}_s[k-1|k-1] + c_h\Delta z_i[k]$ (24)

Prediction cov. $P_s[k|k-1] = P[k-1|k-1] + Q$ (25)

Then, the following mode-matched filtering and likelihood computations are performed for. $j = 1,2,\ldots N_j$:

Meas. prediction $\hat{z}^j\left[k\middle|k-1\right] = \mathbf{p}^T(\hat{x}_s[k|k-1])\mathbf{k}_j + \mathbf{a}^T[k]\mathbf{b}$ (26)

Innovation $\nu^j[k] = z[k] - \hat{z}^j\left[k\middle|k-1\right]$ (27)

Linearized H model $H^j[k] = \left.\frac{dV_o^j(x)}{dx}\right|_{x=\hat{x}_s[k|k-1]}$ (28)

Innovation variance $S^j[k] = R + \left(H^j[k]\right)^2 P_s[k|k-1]$ (29)

Filter gain $W^j[k] = \frac{P_s[k|k-1]H^j[k]}{R + (H^j[k])^2 P_s[k|k-1]}$ (30)

Estimation variance $P_s^j[k|k] = \left(1-W^j[k]H^j[k]\right)^2 P_s[k|k-1] + \left(W^j[k]\right)^2 R$ (31)

Model likelihood $\mathcal{L}^j[k] = \mathcal{N}\left(z[k];\hat{z}^j[k|k-1],S^j[k]\right)$ (32)

Then, the model probabilities are updated as

$$\beta^j[k] = \frac{\mathcal{L}^j[k]\beta^j[k-1]}{\sum_{j=1}^{N_j}\mathcal{L}^j[k]\beta^j[k-1]} \quad (33)$$

Finally, the SOC estimate and the estimation error variance are given by

$$\hat{x}_s[k|k] = \hat{x}_s[k|k-1] + \sum_{j=1}^{N_j}W^j[k]\beta^j[k]\nu^j[k] \quad (34)$$

$$P_s[k|k] = \sum_{j=1}^{N_j}\beta^j[k]\left[P_s^j[k|k] + W^j[k]\left(\nu^j[k]-\bar{\nu}[k]\right)^2\right] \quad (35)$$

Remark: It must be noted that the above procedure is a novel use of the probabilistic data association (PDA) filter from Ref. [24] for the purpose of model identification.

A block diagram of the proposed approach is shown in Fig. 1.

3. Machine learning approach to efficient OCV parameter storage

BFGs in portable applications are preferred to have the ability gauge any battery without strictly requiring offline OCV characterization. This is partly due to the time and cost involved in the OCV characterization process; the possibility of frequent battery changes (including swaps) also make such BFGs very desirable.

It is generally understood that the shape of the OCV curve depends on the chemical and physical structure of the battery. However, there are no analytical expressions for the OCV characterization in terms of chemical and physical structure. In practice, the OCV curves are obtained through offline experimentation. In Ref. [1] we review many existing approaches for OCV parameter estimation trough experiment. It is found that the OCV curves remain unchanged across temperature and that the OCV curves of many batteries by different manufacturers are similar (provided

that the *normalized OCV modeling* approach described in Ref. [1] is followed). Hence, it must be possible for a BFG to store a few sets of OCV parameters and be able to gauge batteries made by many different manufacturers.

In this section, we discuss ways to select the OCV parameters $\{\mathbf{k}_j\}_{j=1}^{N_j}$ that are used in the multimodel BFG. Table 2 shows the details of the battery cells that were used in the experiment; the fourth column titled "Cell Number" indicates the different cells of the same battery type used in the experiment.

The OCV characterization experiment [1] involves the following four sequential steps:

1. Fully charging the battery at room temperature
2. Bringing the battery to test temperature
3. Fully dischargnig the battery at a slow rate (usually a *C*/30 rate) at the test temperature, and
4. Charging the battery back, until full, at a slow rate (usually a *C*/30 rate) at the same test temperature

The approach described in Ref. [1] can be employed to estimate the OCV parameters. The OCV characterization in the above manner was performed at 15 different temperatures from Ref. −25 °C to 45 °C in steps of 5 °C. Hence, a total of $34 \times 15 = 510$ OCV characterization experiments were performed. In Refs. [1], we provide a complete analysis of these OCV experiments.

One of the important findings from Ref. [1] is that the OCV–SOC characterization curve can be made to be the same across temperatures by using the *normalized OCV modeling*. In the normalized OCV modeling, the battery capacity is computed at each temperature and used for the computation of SOC resulting in a *single* OCV–SOC curve across all temperatures. This enables significant savings in OCV parameter storage, i.e., it is sufficient to store a single set of OCV parameters for each battery type and estimate the battery capacity online [2].

In Table 2, we show the estimated OCV parameters for each cell. These parameters can be used to generate the OCV for a particular SOC as

$$V_o(s) = \mathbf{p}(s)^T \mathbf{k} \tag{36}$$

Fig. 2 shows the OCV–SOC curves of cell listed in Table 2. It can be noticed that, regardless of the battery type, many of the OCV curves are similar. Indeed, for many battery types, the differences between their OCV curves are smaller than the error in computing

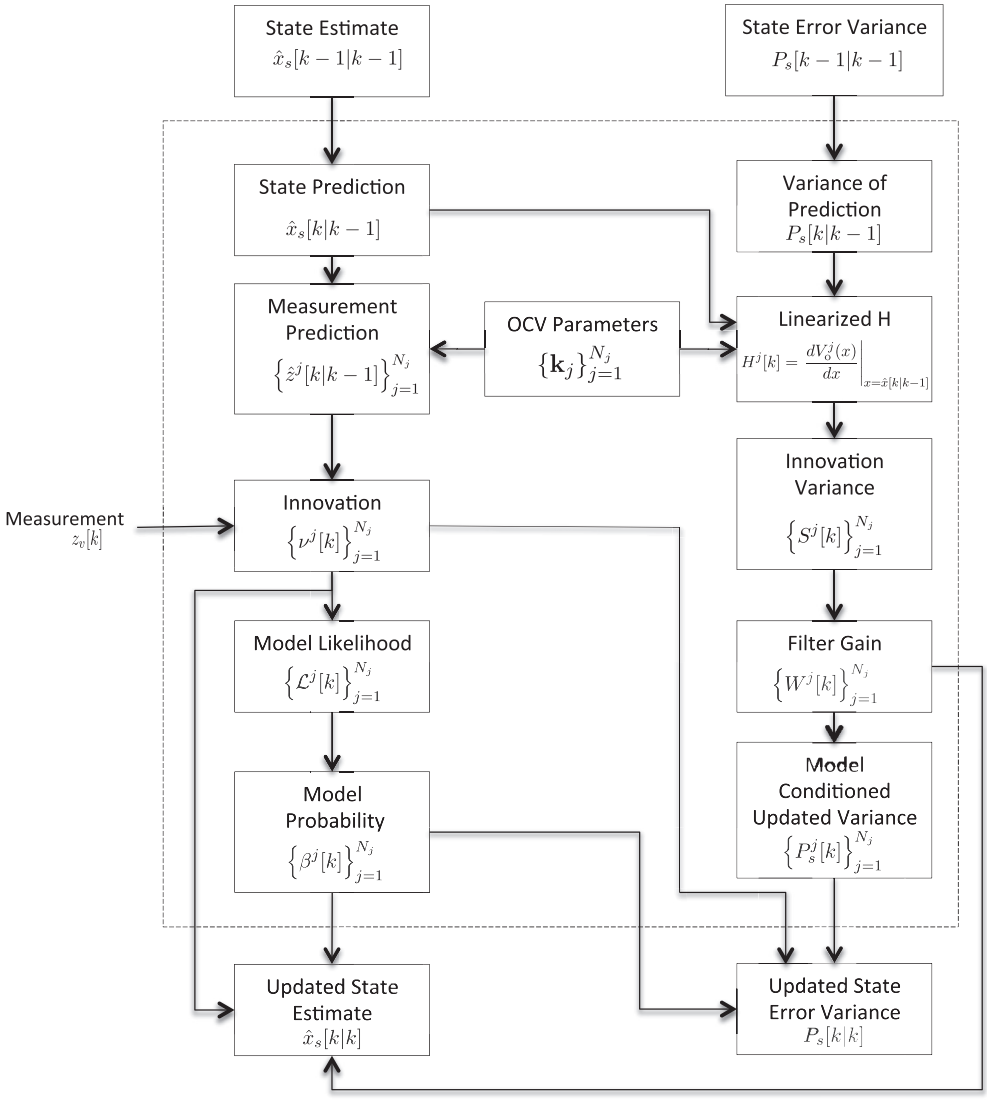

Fig. 1. Block diagram of the proposed multimodel BFG.

Table 2
List of Batteries and their OCV Parameters.

Sample no.	Battery manufacturer	Serial number	Cell number	K0	K1	K2	K3	K4	K5	K6	K7	K8
1	Nokia	BP 4L	1	−4.4813	30.3625	−5.4895	0.6087	−0.0285	−16.9776	38.2121	−0.1162	0.5813
2	Nokia	BP 4L	2	−4.4882	34.7351	−6.1389	0.668	−0.0308	−20.8428	44.9474	−0.1444	0.5581
3	Nokia	BP 4L	3	−5.7439	31.3426	−5.7249	0.6379	−0.0299	−16.2129	38.615	−0.0134	0.5889
4	Nokia	BP 4L	4	−4.1289	45.3504	−7.7859	0.8302	−0.0376	−30.8211	61.2808	−0.3192	0.3708
5	Samsung	EB555157VA	1	−1.5085	41.2402	−7.07	0.7681	−0.0359	−30.3721	57.0893	−0.4572	0.2944
6	Samsung	EB555157VA	2	−2.2216	38.8595	−6.7447	0.7396	−0.0348	−27.3031	52.8784	−0.3599	0.3395
7	Samsung	AB463651	1	−2.7886	36.6116	−6.4458	0.7156	−0.0341	−24.5508	48.9357	−0.2698	0.4056
8	Samsung	AB463651	2	−1.9049	34.9858	−6.1037	0.6732	−0.0319	−24.2116	47.3439	−0.316	0.492
9	Samsung	AB463651	3	−2.3237	47.4112	−8.1229	0.8811	−0.0411	−34.8322	65.6118	−0.4617	0.4508
10	Samsung	AB463651	4	−1.3313	28.2101	−4.8784	0.5292	−0.0247	−18.9233	37.9843	−0.27	0.4251
11	Samsung	EB504465	1	−2.3739	32.6716	−5.784	0.6456	−0.0309	−21.5345	43.4031	−0.2538	0.3799
12	Samsung	EB504465	2	−1.5684	46.4157	−7.9021	0.8536	−0.0397	−34.918	64.8046	−0.5132	0.3358
13	Samsung	EB504465	3	−1.962	33.7161	−5.917	0.656	−0.0313	−23.0268	45.3406	−0.3099	0.3483
14	Samsung	EB504465	4	−1.6756	42.3832	−7.274	0.7917	−0.0371	−31.1357	58.6333	−0.4389	0.356
15	Samsung	EB575152	1	−2.0542	28.6842	−4.9746	0.5372	−0.0249	−18.3279	38.1599	−0.1554	0.6502
16	Samsung	EB575152	2	−1.9791	36.6886	−6.2418	0.6632	−0.0302	−25.6191	50.2428	−0.2748	0.6608
17	Samsung	EB575152	3	−2.5887	36.6903	−6.2908	0.6715	−0.0306	−24.8732	49.677	−0.2402	0.6835
18	Samsung	EB575152	4	−2.9254	25.4594	−4.6864	0.539	−0.0265	−14.3882	32.0363	−0.1311	0.3392
19	Blackerry	FS 1	1	−2.868	19.5393	−3.7414	0.4441	−0.0224	−9.1018	23.1865	−0.0319	0.4245
20	Blackerry	FS 1	2	−1.6544	33.2971	−5.8206	0.6441	−0.0307	−23.0123	45.0151	−0.3222	0.4157
21	Blackerry	M S1	1	−2.2305	24.9583	−4.4232	0.4878	−0.0231	−14.8639	32.3114	−0.1573	0.438
22	Blackerry	M S1	2	−2.1679	25.4322	−4.4909	0.4933	−0.0232	−15.4082	33.0761	−0.1848	0.4029
23	Blackerry	M S1	3	−2.1511	28.6238	−4.9981	0.5446	−0.0255	−18.2572	37.8914	−0.2113	0.4905
24	Blackerry	M S1	4	−0.9741	30.3903	−5.2017	0.5596	−0.0259	−21.3917	41.5533	−0.3517	0.3988
25	LG	LGIP	1	−3.3584	36.5011	−6.4703	0.7216	−0.0344	−23.6683	48.2804	−0.214	0.4695
26	LG	LGIP	3	−2.4388	38.5035	−6.718	0.7406	−0.035	−26.6555	52.1114	−0.3184	0.4415
27	Huawei	HB4Q1	1	−1.6226	39.0734	−6.722	0.732	−0.0343	−28.27	53.7686	−0.4079	0.3679
28	Huawei	HB4Q1	2	−2.4954	35.1997	−6.1698	0.6815	−0.0323	−23.6582	47.1783	−0.2781	0.395
29	Samsung	EBL1A2GBA	1	−1.9747	50.2979	−8.5394	0.9183	−0.0424	−37.858	70.3186	−0.522	0.3504
30	Samsung	EBL1A2GBA	2	−1.8145	50.823	−8.6133	0.9251	−0.0427	−38.5429	71.2411	−0.5464	0.3281
31	Samsung	EBL1A2GBA	3	−1.611	49.5084	−8.3989	0.9035	−0.0418	−37.6603	69.4047	−0.5627	0.2877
32	Samsung	EBL1A2GBA	4	−2.276	49.3495	−8.4102	0.907	−0.042	−36.6127	68.6301	−0.4817	0.3443
33	Samsung	L1G6LLAGS	1	−4.4256	83.6175	−14.0185	1.4878	−0.0678	−64.5844	118.3224	−0.8474	0.3087
34	Samsung	L1G6LLAGS	2	−4.1835	83.7601	−14.0218	1.4864	−0.0676	−65.0311	118.7525	−0.871	0.2839

these curves [1]. Hence, the storage of OCV parameters can be further reduced by selecting curves that represent many similar batteries.

A simple approach to reduce the storage of OCV parameters involves the following steps:

1. *Collect the OCV parameters from as many different battery cells as possible*: It is important to collect the OCV parameters so that they span the envelope of possible OCV–SOC curves. This helps in reducing errors in adaptive BFG. Multiple cells of the same battery in Table 2 serve this purpose.
2. *Cluster the OCV parameters based on similarity*: The similarity of OCV parameters can be simply computed be comparing the OCV parameters of each cell. We compute the Euclidean distance as a measure of dissimilarity, i.e., the *dissimilarity* between $\mathbf{k}_i$ and $\mathbf{k}_j$ is given by

$$d_{ij} = \sqrt{\sum_{s\in[0,1]} \left(\mathbf{p}^T(s)\mathbf{k}_i - \mathbf{p}^T(s)\mathbf{k}_j\right)^2} \tag{37}$$

Fig. 3 shows the dissimilarities of parameters in Table 2 as a dendrogram which is an output of hierarchical clustering [35].

3 *Select one OCV parameter for each cluster*: Once the OCV parameters are grouped, we take the average in each group and store them as the OCV parameter representing that group.[4] This particular parameter is specified as $\mathbf{k}_j$ corresponding to the j^{th} group as used in the multimodel BFG. Fig. 4 shows the three groups found based on the analysis of parameters listed in Table 2. These three groups are labeled as follows: OCV1 – green; OCV2 – red; and OCV3 – blue.

The above approach is summarized in Fig. 5.

4. Simulation results

In this section, we demonstrate the performance of the proposed algorithm on actual battery data. The multimodel BFG is

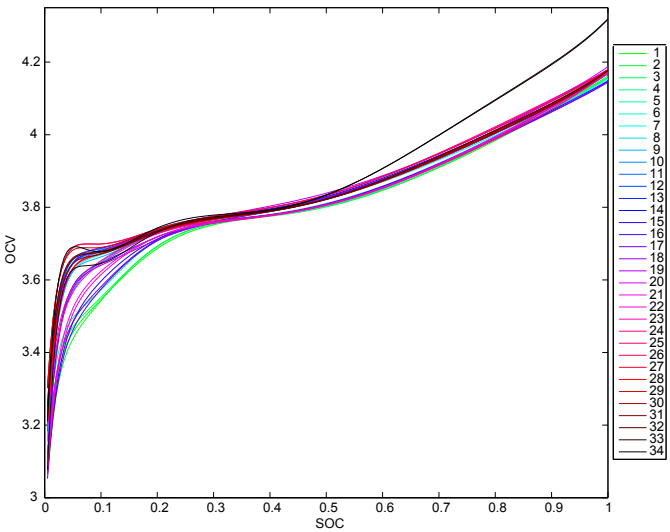

Fig. 2. OCV curves of each battery cell listed in Table 2.

[4] Maximum likelihood combination of OCV parameters is an alternative method.

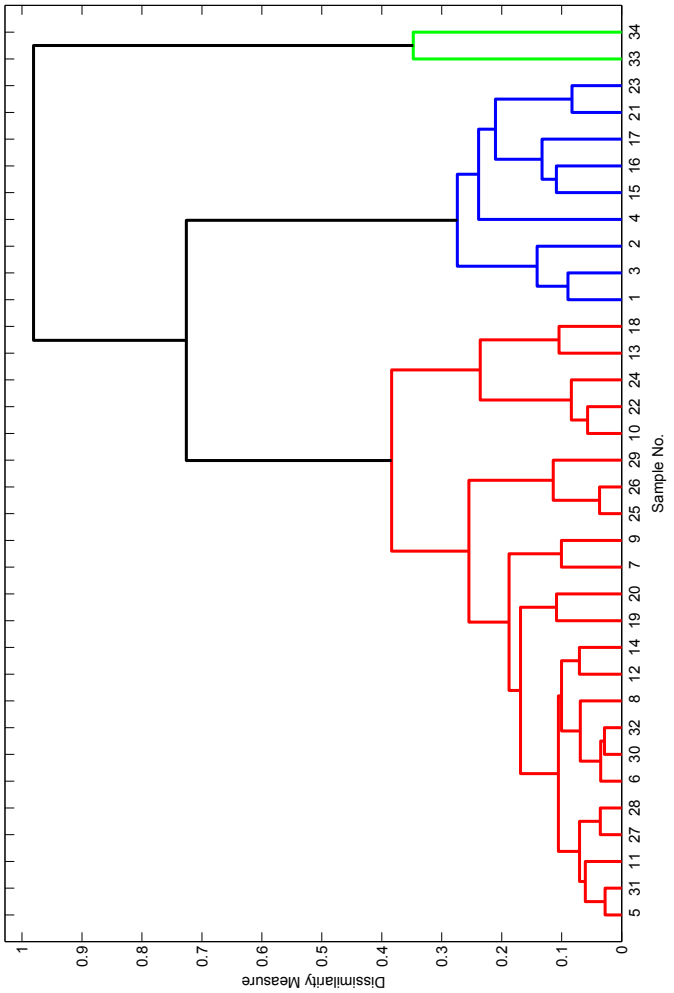

Fig. 3. Hierarchical clustering of OCV curves. Dissimilarity among the OCV parameters are displayed as a dendrogram. It is easy to see three groups of OCV parameters.

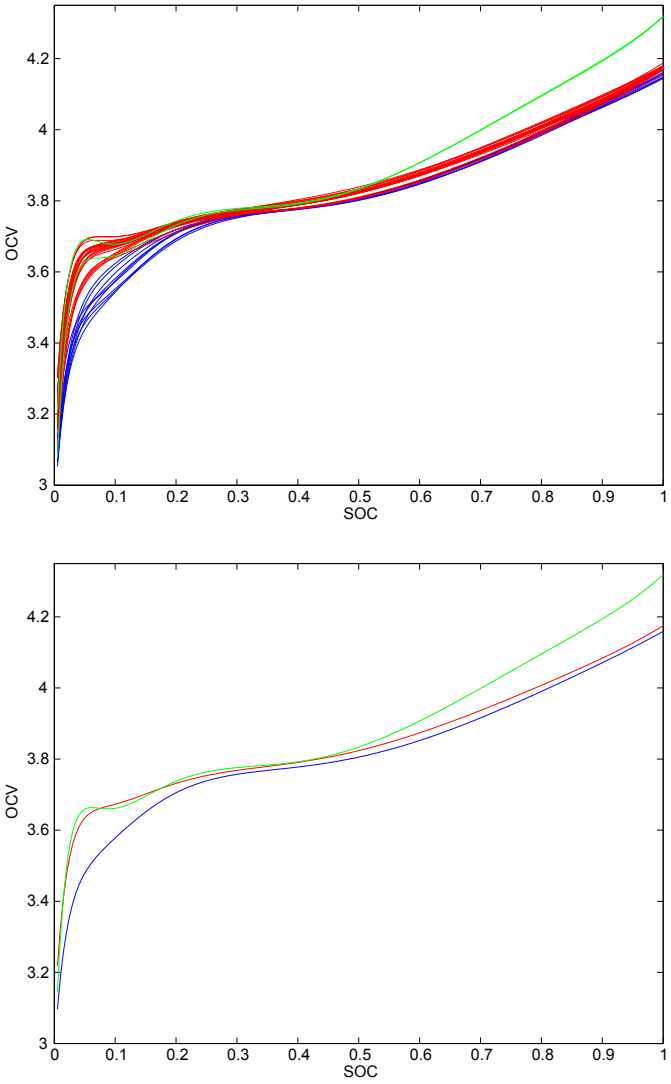

Fig. 4. Grouped OCV curves: The top plot shows the OCV curves corresponding to each group in Fig. 3 in the same color. The plot a the bottom shows the representative OCV plot selected for each group. We label the three plots as follows: OCV1 – green; OCV2 – red; and OCV3 – blue. (For interpretation of the references to color in this figure legend, the reader is referred to the web version of this article.)

equipped with three OCV parameters corresponding to the three curves shown in Fig. 4. For simplicity, we label these curves as OCV1, OCV2 and OCV3. Table 3 summarizes the details of these curves.

The multimodel BFG algorithm proposed in this paper is implemented through state-control in some applications, such as in smart phones, the BFG needs to face such events as battery swaps, new battery replacement and unconventional usage, such as leaving the battery unused until it becomes "dead"; using non-standard chargers that may apply unusual voltages; etc. The state-control [36] checks the voltage and current data for unfavorable conditions (e.g., constant current is not favorable for parameter estimation) and activates, pauses, resets and reactivates different modules of the BFG, such as parameter estimation module, capacity estimation module and SOC tracking module.

Now, we demonstrate the performance of the multimodel BFG through three different examples in the next three subsections.

4.1. Demonstration of PDA in resolving battery type

First, we demonstrate the ability of PDA in BFG to adapt to different battery chemistries without the exact knowledge of the OCV parameters. Fig. 6 shows the data used for this experiment. This data was collected from a Samsung battery with serial number EB575152 as follows: Starting from a fully charged battery, dynamic

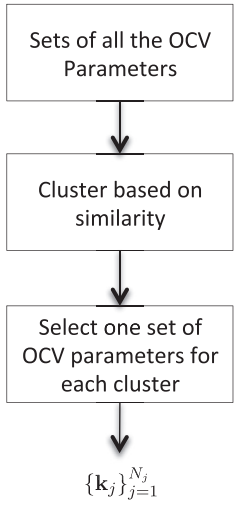

Fig. 5. Proposed approach for efficient parameter storage.

Table 3
Identification of three OCV curves.

Label	Max. OCV	Color/position in Fig. 4
OCV1	4.17 V	Blue/lower
OCV2	4.17 V	Red/middle
OCV3	4.35 V	Green/top

discharge profiles as shown in Fig. 6 (bottom) were applied for 6 h; After that, the batter was charged using a constant current of 750 mA for 30 min; Finally, the dynamic profile was applied until the voltage across the battery terminals reached the shut down voltage of 3 V.

The voltage and current data shown in Fig. 6 were fed to the multimodel BFG algorithm in order to track the battery SOC. The (multimodel) BFG algorithm employs three sets of OCV parameters listed in Table 3. The SOC tracking performance of the multimodel BFG is shown in the bottom of Fig. 7. Initially, the PDA algorithm in the multimodel BFG assigns equal probabilities (1/3) for each OCV model. The correct OCV model corresponding to the input data is identified within (approximately) 1 h of the start of the BFG algorithm — the mode probability of OCV2 rises to 1 in the top plot of Fig. 7.

It must be noted that the BFG algorithm needs an initial "guess" for the SOC at the very start. It can be observed that the initial voltage in the data is approximately 4.17 V (see the top plot of Fig. 6.) The OCV curves OCV1 and OCV2 correspond to 100% SOC at 4.17 V and OCV1 correspond to only 85% SOC at 4.17 V (see the bottom plot of Fig. 4.) The initial SOC guess then becomes. $85 + 100 + 100/3 = 95\%$.

The state-control of the BFG assumes every start of the simulation as the very first time a battery is seen by the BFG. Hence, it takes some time to check for voltage/current patterns before the parameter estimation and PDA are activated. Fig. 8 shows a close up look of the instance when the PDA algorithm starts its computations. The mode probability can be seen updated to the correct value in two steps.

4.2. Demonstration of PDA in portable applications

An important application of multimodel BFG arises in portable battery applications (see Table 1). Consider smartphone scenario

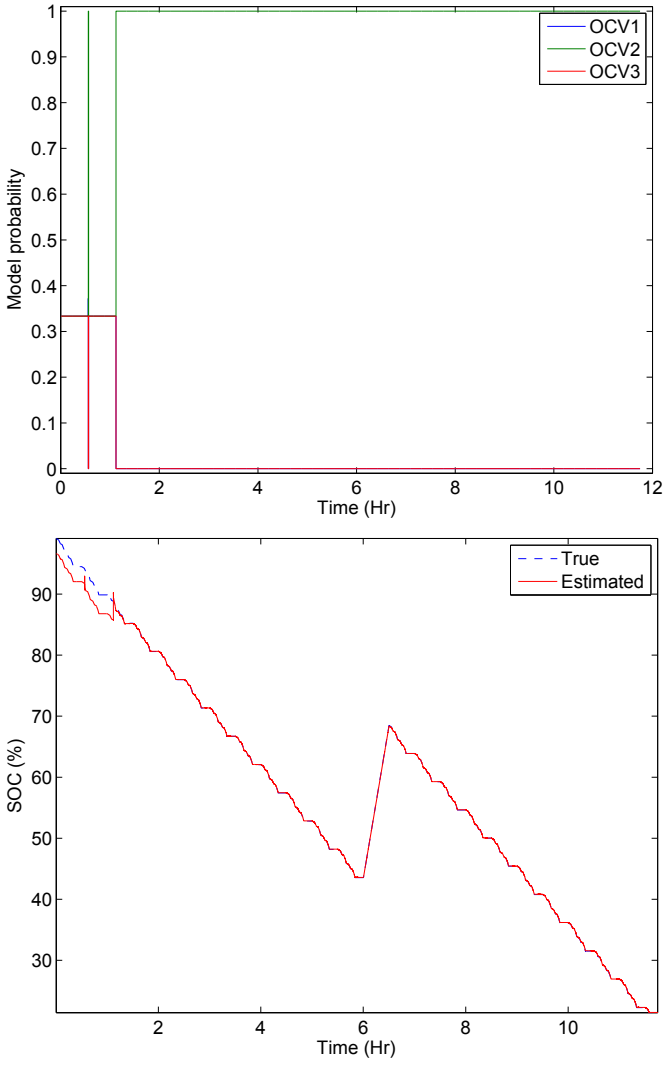

Fig. 7. Demonstration of multimodel BFG in resolving battery type. Initially, the BFG assigns equal probability for the three possible OCV models. Due to the similarity of the OCV1 and OCV2 curves at high SOC region (see bottom of Fig. 4).

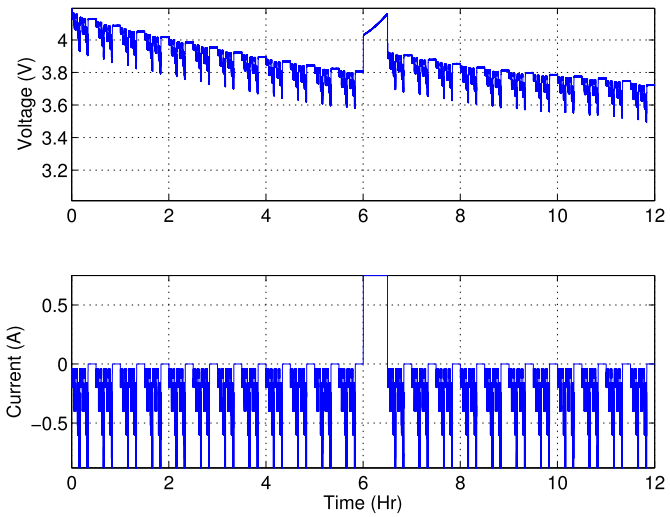

Fig. 6. Voltage and current from the battery. The data is collected from cell 4 of Samsung EB575152 (see Table 2).

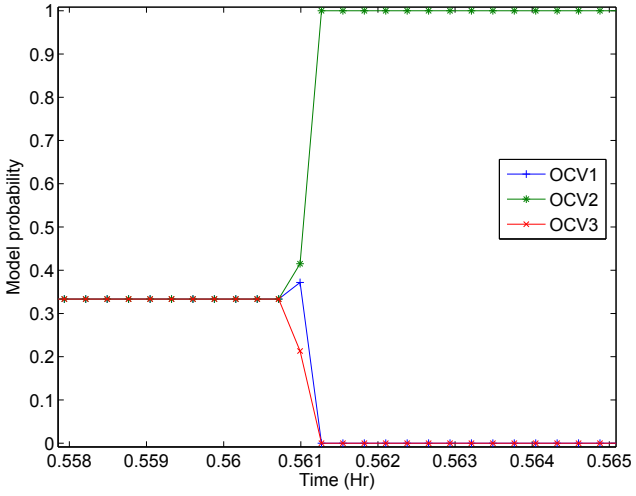

Fig. 8. Mode probability update. Markers indicate the sampling instances. Once the PDA algorithm starts, the accurate mode probability is reached just with two samples (0.2 s).

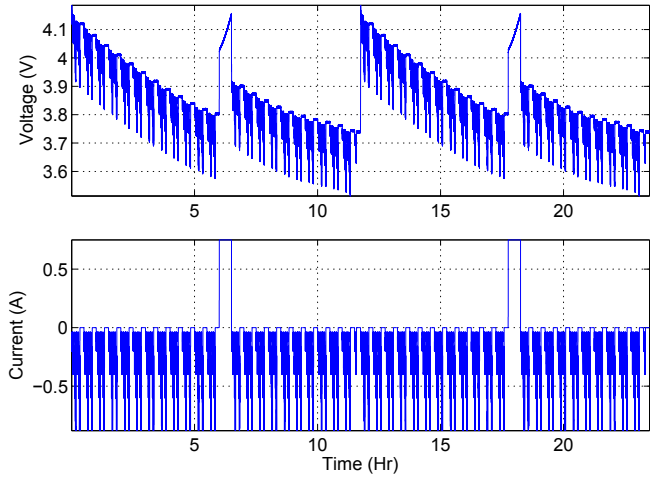

Fig. 9. Battery exchange data in portable applications.

where a user carries a fully charged second (back-up) battery and when the current battery empties it is replaced by the back up battery. Fig. 9 shows the data corresponding to the above battery replacement scenario: The top plot shows that the voltage around the 14 h mark jumping back to full battery voltage with no charging current present. This indicates the scenario that, once the current battery becomes empty, it is replaced by a different battery which might not have the same type of OCV curve.

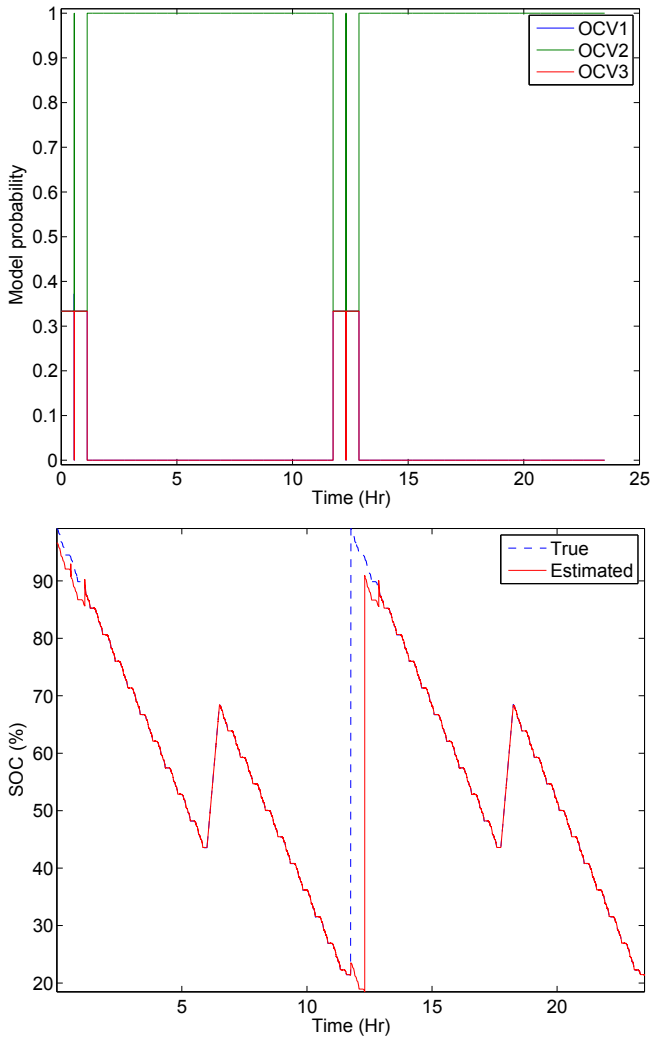

Fig. 10. Demonstration PDA in the replacement scenario.

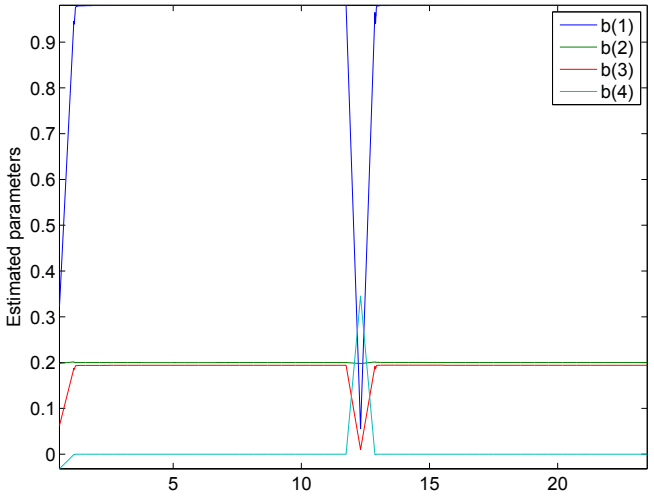

Fig. 11. Estimated parameters in the replacement scenario. A brief dip in estimated parameters can be observed when the new battery is inserted. The state-control of the BFG routinely checks the estimated parameters for instabilities.

Fig. 10 shows the SOC tracking performance of the multimodel BFG and the corresponding mode probability. Similar to the example in Section 4.1, the SOC initialization is obtained by combining the *SOC-lookup* from all OCV curves in the multimodel BFG. The BFG can be similarly reinitialized when a new battery is inserted; however, such reinitialization is not performed in Fig. 10. It can be seen that the BFG is able to adjust to the correct OCV mode within 1 h of processing.

The BFG is implemented with the assumption of a dynamic equivalent model consisting of one series resistor and one RC component; this would result in a 4×1 model parameter vector $\mathbf{b}$ (see Ref. [19] for details). Fig. 11 shows the dynamic battery equivalent model parameter estimates for the example corresponding to Fig. 10. Each element of $\mathbf{b}$ is labeled as $\mathbf{b}(1)$, $\mathbf{b}(2)$, $\mathbf{b}(3)$ and $\mathbf{b}(4)$. It can be seen that the new battery insertion affects the parameter estimates as well.

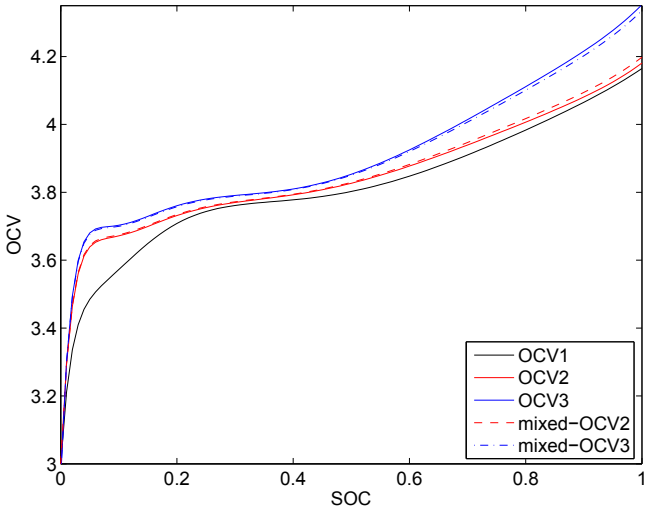

Fig. 12. OCV curves used in simulated PDA experimentation.

Table 4
Parameters of baseline and mixed OCV curves.

	Parameters							
	K0	K1	K2	K3	K4	K5	K6	K7
OCV1	−3.0927	43.3102	−7.4126	0.7908	−0.0359	−30.3610	59.0316	−0.3932
OCV2	−1.2528	49.7952	−8.4537	0.9127	−0.0425	−38.3972	70.0370	−0.6151
OCV3	−2.5215	67.8629	−11.3633	1.2086	−0.0554	−52.9221	96.3480	−0.8136
Mixed-OCV2	−2.2678	64.2493	−10.7814	1.1494	−0.0528	−50.0171	91.0858	−0.7739
Mixed-OCV3	−1.5065	53.4087	−9.0356	0.9719	−0.0451	−41.3022	75.2992	−0.6548

4.3. Demonstration of PDA when the battery chemistry is unknown

This simulated example is designed to demonstrate the ability of the PDA algorithm to find the *closest* OCV parameter set from the library in the absence of exact OCV parameter sets corresponding to the battery being gauged. The mode probability in the PDA algorithm will converge to the closest OCV parameter set that gives the highest likelihood for the data; this phenomenon was proved in Ref. [37].

In Fig. 12, we introduce two more OCV curves in addition to the three *baseline OCV curves* (see the bottom plot in Fig. 4) that we selected through the machine learning approach described in Section 3; parameters for these two additional OCV curves are generated as follows.

$$\mathbf{k}_{\text{mixed}-\text{OCV2}} = 0.8\mathbf{k}_{\text{OCV2}} + 0.2\mathbf{k}_{\text{OCV3}} \tag{38}$$

$$\mathbf{k}_{\text{mixed}-\text{OCV3}} = 0.2\mathbf{k}_{\text{OCV2}} + 0.8\mathbf{k}_{\text{OCV3}} \tag{39}$$

where each $\mathbf{k}$ is an OCV parameter set corresponding to a category indicated in the subscript; the OCV curve corresponding to mixed-OCV2 is more similar to OCV2 than it is to OCV3; and the OCV curve corresponding to mixed-OCV3 is more similar to OCV3 than it is to OCV2. Table 4 lists the OCV parameter sets corresponding to curves denoted as OCV1, OCV2, OCV3, mixed-OCV2 and mixed-OCV3 in Fig. 12.

Now, we will test the PDA-BFG by feeding it with data generated based on different OCV curves shown in Fig. 12. Detailed descriptions of how to simulate battery data are discussed in Refs. [2,19,20]. In short, first the true SOC is computed based on an assumed battery capacity and known initial SOC (we use $s[0] = 1$) for a dynamic current profile similar to the one shown in Fig. 6; then, the observation model (2) is used to generate voltage measurements with an assumed voltage measurement error s.d. of $\sigma_v = 1$ mV and current measurement error s.d. of $\sigma_v = 1$ mA.

First, we demonstrate the expected SOC tracking performance when the exact OCV parameters of the battery being gauged is known to the BFG. Fig. 13 shows the summary of results for this scenario; the battery data was simulated using the parameters of OCV3 curve in Fig. 12; the PDA-BFG algorithm has the OCV parameters corresponding to curves labeled OCV1, OCV2 and OCV3 in Fig. 12. The top plot in Fig. 13 shows the mode probability quickly converging towards the correct OCV model; the second and third plots show the SOC tracking error quickly converging towards zero.

In Fig 14, the SOC tracking performance of the PDA-BFG in the absence of the exact OCV parameter is demonstrated. The battery data was simulated using the parameters of mixed-OCV2 curve in Fig. 12; as before, the PDA-BFG algorithm has only the OCV parameters corresponding to curves labeled OCV1, OCV2 and OCV3 in Fig. 12. The parameters of mixed-OCV2 is more similar to OCV2 than any other OCV parameters in the library (see (38)); as such, the mode probability (top plot) of PDA-BFG quickly converges towards OCV2. The SOC tracking error is not zero (but small enough – less than 1%) due to the fact that the OCV2 curve is close but not the same as that of mixed-OCV2.

Fig 15 shows a similar mismatched OCV simulation and the corresponding results from the PDA-BFG algorithm; in this figure, the data is generated based on mixed-OCV3.

5. Conclusions

We presented a novel approach for battery fuel gauging that is able to adapt to many different battery chemistries. We showed

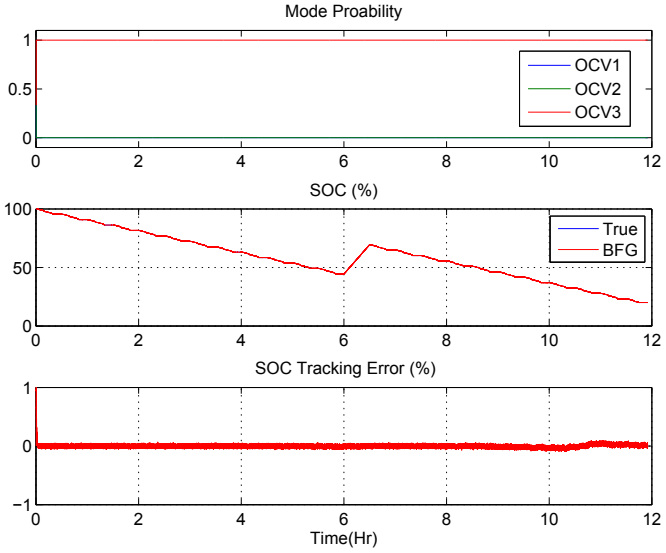

Fig. 13. Demonstration of PDA-BFG on simulated data. The data is generated based on the parameters of OCV3 which is available in the parameter library of PDA-BFG.

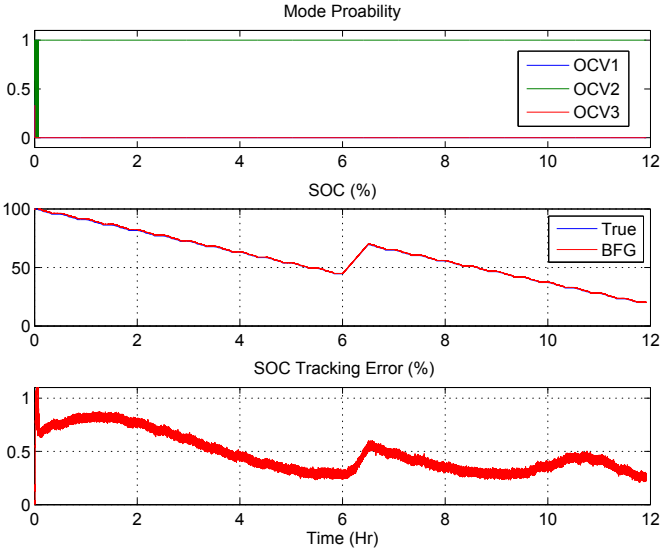

Fig. 14. Demonstration of PDA-BFG on simulated data. The data is generated based on the parameters of mixed-OCV2 which is not available in the parameter library of PDA-BFG.

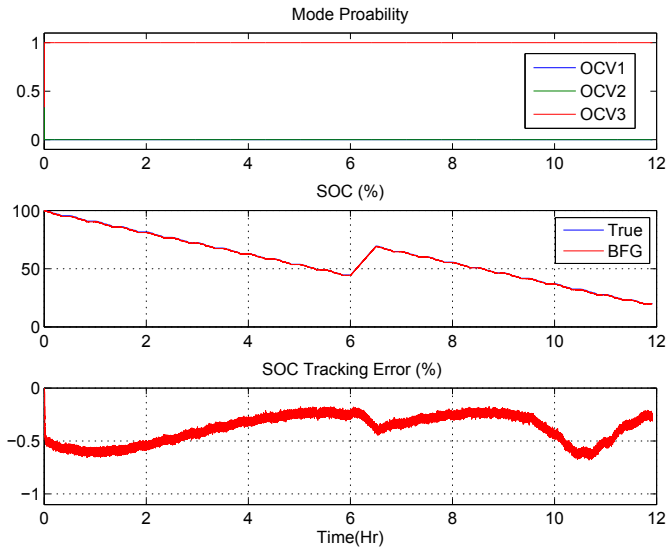

Fig. 15. Demonstration of PDA-BFG on simulated data. The data is generated based on the parameters of mixed-OCV3 which is not available in the parameter library of PDA-BFG.

in a recent work [1], via *normalized OCV modeling*, that the OCV characterization curve does not change with the temperature of the cell – which enables battery fuel gauging (BFG) with a single OCV curve regardless of the temperature. In this paper, we show that the (normalized) OCV curves of batteries from many different manufacturers are similar. Based on this observation, and by using machine learning algorithms, we develop an approach to analyze a large number of OCV parameters (representing many different batteries) and to select a few sets of parameters that are representative of the entire set of batteries. The proposed multimodel BFG approach then uses those selected OCV parameters and the probabilistic data association (PDA) algorithm in order to associate the battery to the correct OCV model, i.e., identify it. The resulting multimodel BFG can be used to gauge a wide range of batteries without requiring battery-specific OCV parameters.

Acknowledgments

We thank the anonymous reviewers for providing useful comments and suggestions that resulted in the improved quality of this paper. We would like to thank Prof. Gregory L. Plett of University of Colorado at Colorado Springs for the collection of the experimental data used in this paper. The work reported in this paper was partially supported by National Science Foundation grants ECCS-0931956 (NSF CPS), ECCS-1001445 (NSF GOALI), CCF-1331850 (Cyber SEES), Army Research Office grant W911NF-10-1-0369, and ONR grant N00014-10-1-0029. We thank NSF, ARO and ONR for their support of this work. Y. Bar-Shalom was partially supported by Grant ARO W911NF-10-1-0369. Any opinions expressed in this paper are solely those of the authors and do not represent those of the sponsors.

Appendix A. Supplementary data

Supplementary data related to this article can be found at http://dx.doi.org/10.1016/j.jpowsour.2014.09.006.

References

[1] B. Pattipati, B. Balasingam, G. V. Avvari, K. Pattipati, Y. Bar-Shalom, J. Power Sources 269 (317–333).
[2] B. Balasingam, G. V. Avvari, B. Pattipati, K. R. Pattipati, Y. Bar-Shalom, J. Power Sources, http://dx.doi.org/10.1016/j.jpowsour.2014.07.032.
[3] G.L. Plett, J. Power Sources 134 (2) (2004) 252–261.
[4] G.L. Plett, J. Power Sources 134 (2) (2004) 262–276.
[5] G.L. Plett, J. Power Sources 134 (2) (2004) 277–292.
[6] G.L. Plett, J. Power Sources 161 (2) (2006) 1356–1368.
[7] G.L. Plett, J. Power Sources 161 (2) (2006) 1369–1384.
[8] M. Mastali, J. Vazquez-Arenas, R. Fraser, M. Fowler, S. Afshar, M. Stevens, J. Power Sources 239 (2013) 294–307.
[9] B. Bhangu, P. Bentley, D. Stone, C. Bingham, Veh. Technol. IEEE Trans. 54 (3) (2005) 783–794.
[10] I.-S. Kim, J. Power Sources 163 (1) (2006) 584–590.
[11] J. Lee, O. Nam, B. Cho, J. Power Sources 174 (1) (2007) 9–15.
[12] S. Lee, J. Kim, J. Lee, B. Cho, J. Power Sources 185 (2) (2008) 1367–1373.
[13] J. Kim, B.-H. Cho, Veh. Technol. IEEE Trans. 60 (9) (2011) 4249–4260.
[14] J. Kim, S. Lee, B. Cho, J. Power Sources 196 (4) (2011) 2227–2240.
[15] S. Chen, Y. Fu, C. Mi, State of Charge Estimation of Lithium Ion Batteries in Electric Drive Vehicles Using Extended Kalman Filtering.
[16] H. He, R. Xiong, X. Zhang, F. Sun, J. Fan, Veh. Technol. IEEE Trans. 60 (4) (2011) 1461–1469.
[17] C. Hu, B.D. Youn, J. Chung, Appl. Energy 92 (2012) 694–704.
[18] X. Hu, F. Sun, Y. Zou, Energies 3 (9) (2010) 1586–1603.
[19] B. Balasingam, G. V. Avvari, B. Pattipati, K. R. Pattipati, Y. Bar-Shalom, J. Power Sources, http://dx.doi.org/10.1016/j.jpowsour.2014.07.034.
[20] B. Balasingam, G.V. Avvari, B. Pattipati, K.R. Pattipati, Y. Bar-Shalom, J. Power Sources (2014) under review.
[21] H. He, X. Zhang, R. Xiong, Y. Xu, H. Guo, Energy 39 (1) (2012) 310–318.
[22] R. Xiong, F. Sun, X. Gong, C. Gao, Appl. Energy 113 (2014) 1421–1433.
[23] Y.-H. Chiang, W.-Y. Sean, J.-C. Ke, J. Power Sources 196 (8) (2011) 3921–3932.
[24] Y. Bar-Shalom, P. K. Willett, X. Tian, Tracking and Data Fusion, a Handbook of Algorithms. Yaakov Bar-Shalom.
[25] H. Barth, C. Schaeper, T. Schmidla, H. Nordmann, M. Kiel, H. Van der Broeck, Y. Yurdagel, C. Wieczorek, F. Hecht, D.U. Sauer, Development of a universal adaptive battery charger as an educational project, in: IEEE Power Electronics Specialists Conference, 2008, pp. 1839–1845.
[26] H.-H. Hussein, I. Batarseh, IEEE Trans. Veh. Technol. 60 (3) (2011) 830–838.
[27] H.-H. Hussein, M. Pepper, A. Harb, I. Batarseh, An efficient solar charging algorithm for different battery chemistries, in: IEEE Vehicle Power and Propulsion Conference, 2009, pp. 188–193.
[28] S.-Y. Park, H. Miwa, B.T. Clark, D. Ditzler, G. Malone, N.S. D'souza, J.-S. Lai, A universal battery charging algorithm for ni-cd, ni-mh, sla, and li-ion for wide range voltage in portable applications, in: IEEE Power Electronics Specialists Conference, 2008, pp. 4689–4694.
[29] A. Abdollahi, X. Han, G.V. Avvari, N. Raghunathan, B. Balasingam, K.R. Pattipati, Y. Bar-Shalom, J. Power Sources (2014) under review.
[30] A. Abdollahi, X. Han, N. Raghunathan, B. Balasingam, K.R. Pattipati, Y. Bar-Shalom, J. Power Sources (2014) under review.
[31] A. Abdollahi, N. Raghunathan, B. Pattipati, X. Han, B. Balasingam, K.R. Pattipati, Y. Bar-Shalom, J. Power Sources (2014) under review.
[32] D.F. Crouse, P. Willett, K. Pattipati, L. Svensson, A look at gaussian mixture reduction algorithms, in: Proceedings of the 14th International Conference on Information Fusion, 2011, pp. 1–8.
[33] A.R. Runnalls, Kullback-Leibler approach to gaussian mixture reduction, IEEE Trans. Aerosp. Electron. Syst. 43 (3) (2007) 989–999.
[34] Y. Bar-Shalom, X.R. Li, T. Kirubarajan, Estimation with Applications to Tracking and Navigation: Theory Algorithms and Software, John Wiley & Sons, 2004.
[35] MATLAB, Version 7.13.0.564 (R2011b), The MathWorks Inc., Natick, Massachusetts, 2011.
[36] G. V. Avvari, B. Pattipati, B. Balasingam, K. Pattipati, Y. Bar-Shalom, Battery fuel gauge hardware-in-the-loop validation on li-ion batteries, submitted for publication, IEEE Transactions on Instrumentation and Measurements.
[37] Y. Baram, N.R. Sandell, Automatic Control, IEEE Trans. 23 (3) (1978) 451–454, http://dx.doi.org/10.1109/TAC.1978.1101745.